THE JOURNAL OF PHYSICAL CHEMISTRY C

Article

pubs.acs.org/JPCC

Direct Zircon-to-Scheelite Structural Transformation in YPO_4 and $YPO_4:Eu^{3+}$ Nanoparticles Under High Pressure

Hongsheng Yuan,[†] Kai Wang,[†] Shourui Li,[†] Xiao Tan,[†] Qian Li,[†] Tingting Yan,[†] Benyuan Cheng,[†] Ke Yang,[‡] Bingbing Liu,[†] Guangtian Zou,[†] and Bo Zou.*[,†]

[†]State Key Laboratory of Superhard Materials, Jilin University, Changchun 130012, China

[‡]Shanghai Institute of Applied Physics, Chinese Academy of Sciences, Shanghai 201203, China

ABSTRACT: The high-pressure behavior of zircon-structured YPO_4 (with/without Eu^{3+} doping) nanoparticles was examined at room temperature using in situ synchrotron X-ray diffraction (XRD) and photoluminescence (PL) measurements. In contrast with the reported XRD results of bulk YPO_4 upon compression, the nanoparticles showed a distinct transition sequence: zircon phase → scheelite phase (~18 GPa) without the metastable monazite phase. By the return to ambient pressure, both XRD and PL results revealed that the scheelite phase could be reserved. Further Raman experiments helped us to identify the valuable mode $\nu_1(A_g)$ of the scheelite structure in the quenched samples. The dopants effect, quasi-hydrostatic stress, and nanoscale-induced surface energy difference are considered to explain the high-pressure behavior of the nanoparticles. It is proposed that the nanoscale-induced higher surface energy contribution plays a crucial role in the distinctive high-pressure behavior of the nanoparticles.

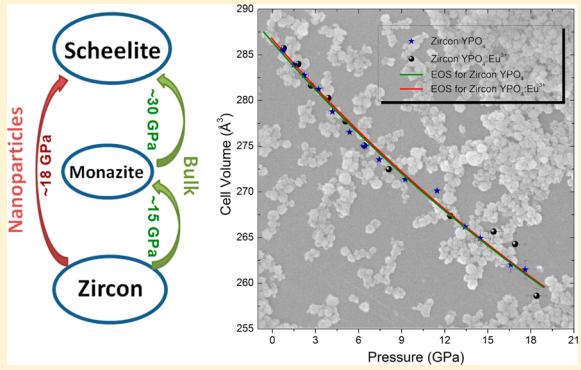

INTRODUCTION

As common accessory minerals, zircon [space group (SG): $I4_1/amd$, $Z = 4$] structured ABO_4 ternary oxides are very important materials from both a theoretical and a technological point of view.[1] The zircon-to-scheelite [SG: $I4_1/a$, $Z = 4$] phase transition is very common in these minerals, and it is of broad interest in geophysics and geochemistry due to the applications in studies on the evolution of Earth's crust and mantle as well as on age dating.[1,2] Therefore, a significant amount of research work on the high-pressure behavior of zircon-structured ABO_4 compounds has been carried out by X-ray diffraction (XRD),[1,3−12] Raman,[1,3,6,13−21] and photoluminescence (PL)[1,16,22−25] spectroscopic experiments as well as by theoretical calculations[6,26−28] in the last decades. Among the ABO_4 ternary oxides, trivalent rare-earth orthophosphates RPO_4 generally crystallize, depending on the ionic radii of the R cation, in two different structural types: zircon and monazite [SG: $P2_1/n$, $Z = 4$]. Those with a small R size ($r_R < r_{Gd}$) adopt the zircon structure under ambient conditions, whereas the other orthophosphates have the lower-symmetry monoclinic monazite structure.[5,29] Specifically, depending on the growth conditions, $GdPO_4$, $TbPO_4$, $DyPO_4$, and $HoPO_4$ can adopt either zircon or monazite structure.[30] Zircon structure can be viewed as being composed of alternating edge-sharing RO_8 dodecahedra and PO_4 tetrahedra arranged in linear chains along the c axis.[5,29] In monazite structure, a ninth oxygen is introduced to form RO_9 polyhedra for the large R cation. The larger R cation causes structural distortions, specifically a rotation of the PO_4 tetrahedra and a lateral shift of the (100) plane, thereby reducing the symmetry from $I4_1/amd$ to $P2_1/n$.[5]

The high-pressure behavior of zircon RPO_4 compounds was addressed recently. Upon compression, those compounds where the R/P cation size ratio is similar to that of monazite prefer the zircon-to-monazite phase transition, and those where the R/P cation size ratio is similar to that of scheelite prefer the zircon-to-scheelite phase transition.[5] For instance, Stavrou et al. carried out high-pressure experiments of $TmPO_4$ using XRD and Raman measurements recently.[3] The results revealed a pressure-induced zircon-to-scheelite transition at 20 GPa. Most notably, at the same transition pressure, the monazite phase was also detected at a low concentration, which decreased and eventually vanished upon further compression. A borderline case for $TmPO_4$ was proposed to understand the results.

It is well known that the thermodynamic properties of nanomaterials may differ significantly from their bulk counterparts due to large surface-to-volume ratio.[31] Therefore, it is appealing to investigate how extreme conditions of pressure contribute to phase transition behaviors in the nanomaterials. To our best knowledge, there is no high-pressure study about the RPO_4 compounds on the nanoscale. Furthermore, a small number of Eu^{3+} ions substituting for the R^{3+} ions in these compounds are very sensitive to the symmetry of their local site, so the PL properties of these compounds are considerably

Received: September 7, 2012
Revised: October 25, 2012
Published: November 2, 2012

dx.doi.org/10.1021/jp3088995 | J. Phys. Chem. C 2012, 116, 24837−24844

affected by pressure. As a common accessory mineral in plutonic and metamorphic rocks, the mineral xenotime (YPO_4) has gained increasing attention recently due to its wide potential application and interesting optical and luminescence properties.[32,33] In previous high-pressure reports, the zircon-to-monazite(-to-scheelite) transition was investigated in bulk YPO_4,[5,6] and hence it is of great interest to explore the structural stability of the three phases for YPO_4 on nanoscale.

In this study, in situ high-pressure investigations of Eu-doped YPO_4 (YPO_4:Eu^{3+}) nanoparticles by XRD and PL experiments have been reported. To clarify, in situ high-pressure XRD experiments on the YPO_4 nanoparticles were conducted as well. Further Raman measurements were performed for the quenched YPO_4:Eu^{3+} samples, and the valuable Raman mode $\nu_1(A_g)$ of the scheelite phase was identified. Convincing experimental evidence showed that the YPO_4(:Eu^{3+}) nanoparticles transform from the original zircon phase to scheelite phase near 18 GPa without undergoing the transition to the metastable monazite structure. This special high-pressure behavior in YPO_4(:Eu^{3+}) nanoparticles have been discussed from many aspects, and the nanoscale-induced surface energy difference could best explain this unusual behavior. From the viewpoint of practical application, we proposed an optimizing feasible synthetic path to attaining new structural technologically relevant materials with tailored properties by virtue of the nanoscale-induced effect.

EXPERIMENTAL SECTION

The YPO_4 and the YPO_4:Eu^{3+} (5 mol % Eu) samples were prepared by a hydrothermal method according to the reported procedure.[32,33] The scanning electron microscopy image (JEOL JEM-6700F) revealed that the as-synthesized nanocrystals were uniform with particle-like morphology and with a diameter of 50−100 nm, as shown in Figure 1.

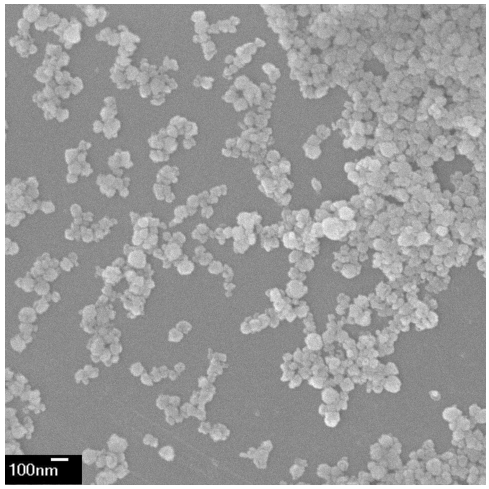

Figure 1. SEM images of particle-like YPO_4:Eu^{3+} nanocrystals.

High-pressure experiments were conducted in a symmetric diamond anvil cell (DAC) furnished with 300 μm culet diamonds. The sample was placed in the 110 μm diameter holes of the T301 steel gasket, which was preindented to the thickness of 35 μm. A small ruby chip was inserted into the sample compartment for in situ pressure calibration, utilizing the R_1 ruby fluorescence method.[34] The 4:1 mixture of methanol and ethanol was used as pressure-transmitting medium (PTM). In situ high-pressure angle-dispersive XRD experiments with a wavelength of 0.6199 Å and a focused beam size of ∼4 × 7 μm^2 were performed at beamline 15U1, Shanghai Synchrotron Radiation Facility (SSRF), China. The XRD patterns were collected for 10 s at each pressure using a Mar-165 CCD detector and then were integrated with FIT2D program.[35] A detailed Rietveld analysis was performed using the GSAS software with the graphical EXPGUI user interface.[36] In situ PL measurements under high pressure were performed with a Quanta Master 40 spectrometer (produced by Photon Technology) in reflection mode.[37−39] The 405 nm line of a violet diode laser with a spot size of 20 μm and a power of 30 mW was used as the excitation source. The typical resolution in the present study was 0.25 nm, and the normalized intensity of all measured peaks in PL spectra was recorded. The Raman scattering measurements were carried out using the Renishaw system (inVia Raman microscope) with a 632.8 nm He−Ne laser as the excitation source. The laser power was 10 mW at the sample, and the integration time was 50 s. The resolution of Raman system was ∼1 cm^{-1}.

RESULTS AND DISCUSSION

The pressure evolution of the angle-dispersive XRD patterns of the YPO_4:Eu^{3+} nanoparticles is shown in Figure 2a. Apart from pressure-induced shifts and quasi-hydrostatic stress-induced broadening of the Bragg peaks, the diffraction patterns do not change significantly up to 16.9 GPa. All observed peaks in this pressure range can be indexed as zircon structure. With further increase in pressure, a new broad peak with a shoulder at diffraction angle around 12.6° marked with arrows appears clearly in the patterns after 18.4 GPa, thus indicating the onset of a phase transition. This peak becomes stronger at higher pressures, and more of the sample transforms to the high-pressure phase(s). The following analysis indicates that the broad peak is the strongest diffraction maxima of (013) and (112) of the scheelite structure. The Bragg peaks marked by the arrows and solid circles in Figure 1 can be readily attributed to the diffractions of the scheelite and zircon structure, respectively. When the pressure approaches 32.4 GPa, the zircon phase is still detected. The high-pressure phase together with zircon phase is quenched upon complete decompression. In addition, the zircon-to-scheelite phase transition is sluggish in the YPO_4:Eu^{3+} nanoparticles, and this sluggishness has also been observed in zircon $LuPO_4$ compounds because of the displacive phase-transition nature.[12]

High-pressure XRD experiments were reported for the bulk YPO_4 compounds, and different kinds of PTM were applied. Errandonea et al.[5] investigated a reversible zircon-to-monazite transition at 19.7 GPa with neon as PTM up to 28 GPa; Zhang et al.[6] detected a zircon-to-monazite-to-scheelite transition using methanol/ethanol mixture as PTM. With the increasing pressure, the zircon-to-monazite transition pressure is ∼15 GPa, followed by monazite-to-scheelite transition at ∼30 GPa. If the high-pressure low-symmetry monoclinic monazite structure existed, then there should be many corresponding Bragg peaks (011, 101, 200, 020, 111, 002, 130, 131) in a large pressure range, not overlapping significantly with zircon or scheelite peaks positions. However, we have not observed any change that could prove the occurrence of monazite structure in the diffraction patterns (Figure 2a), indicating the direct zircon-to-scheelite transition without a postmonazite modification like almost all RVO_4 (R = rare earth) materials.[8,10,14−17,19,20,22] The question is raised, "what changes the

dx.doi.org/10.1021/jp3088995 | J. Phys. Chem. C 2012, 116, 24837−24844

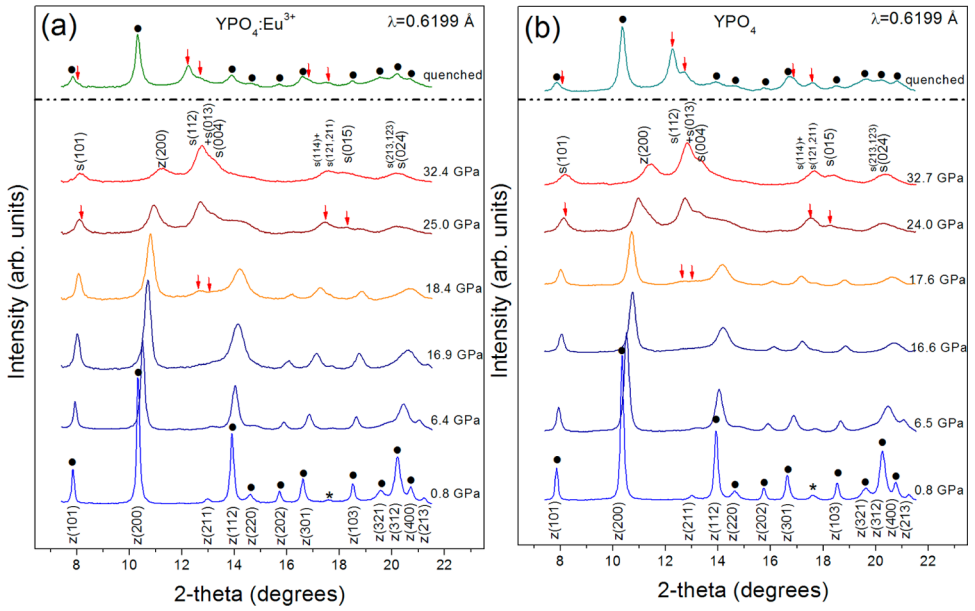

Figure 2. X-ray diffraction patterns of $YPO_4:Eu^{3+}$ nanoparticles (a) and YPO_4 nanoparticles (b) at various pressures. The arrows and solid circles denote Bragg peaks attributed to the scheelite and zircon phases, respectively. The asterisks denote Bragg peaks due to the stainless-steel gasket.

phase transition sequence in $YPO_4:Eu^{3+}$ nanoparticles?". Bearing in mind this intriguing question, subsequent experiments and analysis were carried out.

In our case, the major peak broadening results from quasi-hydrostatic stress presented in the ethanol−methanol as PTM above its solidification pressure (~10 GPa). With respect to the bulk YPO_4 compounds, the metastable monazite phase is detected apparently not only under hydrostatic conditions but also under quasi-hydrostatic conditions.[5,6] So, we propose that quasi-hydrostatic conditions could not affect the transition sequence or at least could not play a crucial role for the nanoparticles.

Furthermore, we would like to check whether the small amounts of dopants affect structure stability, which is proven to play a crucial role in high-pressure-induced phase transitions of Y_2O_3 and $Y_2O_3:Eu^{3+}$.[40] Accordingly, an additional XRD experiment was performed for pure YPO_4 nanoparticles. The typical XRD patterns of YPO_4 nanoparticles at various pressures are shown in Figure 2b. Apart from a somewhat lower transition pressure (~17.6 GPa), the pressure-induced phase transition is the same as that of $YPO_4:Eu^{3+}$ nanoparticles. As such, we conclude that the small amounts of dopants (5% Eu^{3+}) do not affect the sequence of the pressure-induced phase transition. Similar to $GdVO_4:Eu^{3+}$ microcrystals,[16] Eu^{3+} doping in YPO_4 has less influence on structure stability than that in Y_2O_3, which is probably related to special cation distribution and the packing style.[40]

Here we analyze the diffraction patterns by performing Rietveld refinements. Typical refined profiles for $YPO_4:Eu^{3+}$ are shown in Figure 3 for (a) 0.8 GPa, pure zircon phase and (b) quenched sample, mixture of scheelite and zircon phases. Because of the serious peak broadening after phase transition, attempts to refine the mixture of zircon and scheelite patterns were unsuccessful. The profiles before the phase transition were refined for both samples.

The pressure dependence of the decreasing a and c lattice parameters together with axial ratio c/a is depicted in Figure 4. We find that the decrease in a and c is linear with linear coefficients of $-1.4(1.5) \times 10^{-2}$ Å/GPa and $-4.0(3.0) \times 10^{-3}$

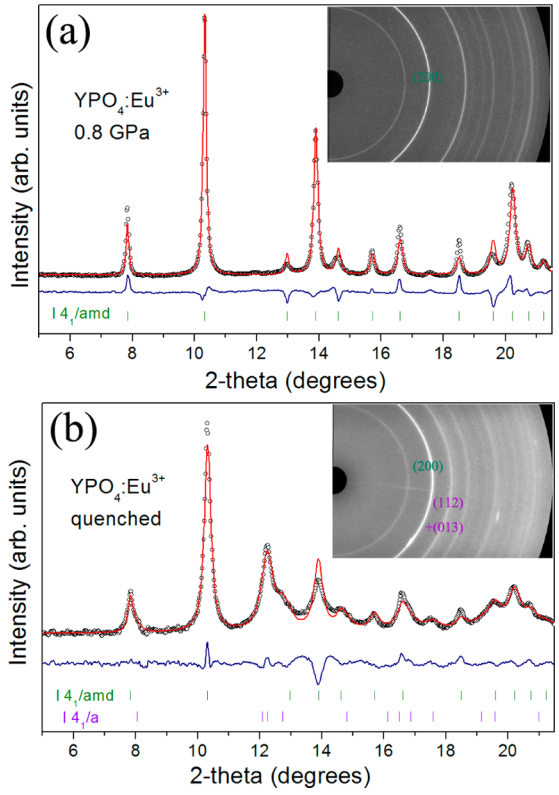

Figure 3. Rietveld refinements for $YPO_4:Eu^{3+}$ nanoparticles at (a) 0.8 GPa, pure zircon structure and (b) quenched sample, mixture of scheelite and zircon structure. The insets represent corresponding diffraction images. The most pronounced diffractions in the two phases are marked in the images with different colors.

Å/GPa for $YPO_4(:Eu^{3+})$ nanoparticles, respectively, so that the a axis is more compressible than the c axis. As a consequence, the axial ratio c/a increases from ~0.87 at 0.8 GPa to ~0.90 near 18 GPa, approaching the axial ratio of $ZrSiO_4$ (0.906). A similar behavior has been previously found in bulk $TmPO_4$

dx.doi.org/10.1021/jp3088995 | J. Phys. Chem. C 2012, 116, 24837−24844

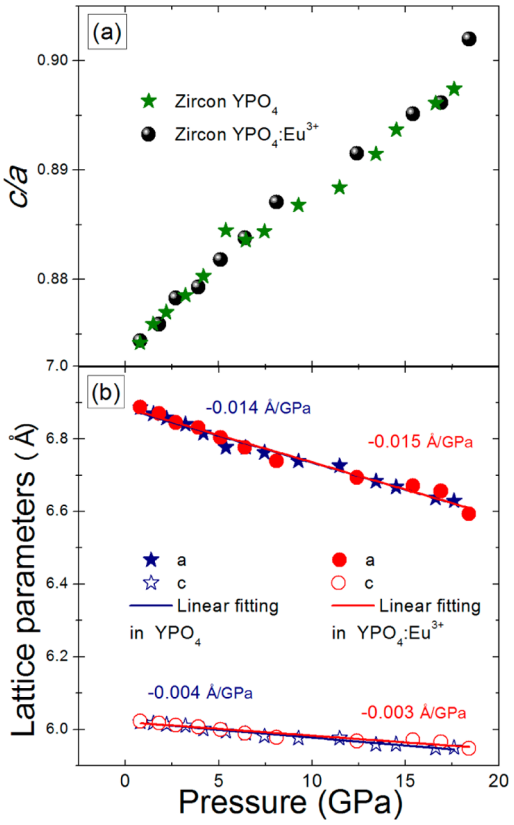

Figure 4. Axial ratio and lattice constants for the zircon phase of YPO_4(:Eu^{3+}) nanoparticles as a function of pressure.

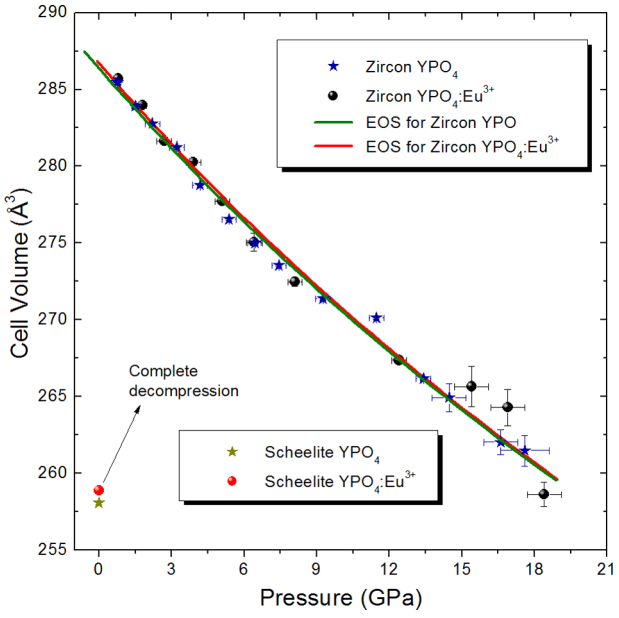

Figure 5. Volume−pressure data for the zircon and scheelite phases of YPO_4(:Eu^{3+}) nanoparticles.

compounds.[3] Also, isomorphic compounds such as YVO_4 show the same anisotropic compressibility.[10] The origin of this behavior is related to the packing of RO_8 and $P(V)O_4$ polyhedra in the zircon structure, which is discussed by Errandonea et al. in detail.[1,5,9] In addition, there is only one crystallographically distinct site for the Y atoms in the crystal structure of zircon YPO_4, and both the Eu^{3+} and Y^{3+} ions have the same valence and atomic radius, resulting in no charge compensation issues in YPO_4:Eu^{3+}. Therefore, small Eu^{3+} substitution (5%) for Y^{3+} makes a quite similar compressibility of the unit-cell parameters in the zircon YPO_4:Eu^{3+} and YPO_4 nanoparticles.

The unit-cell volumes are shown in Figure 5. By fitting the third-order Birch−Murnaghan equation of state, the following results are given: V_0 = 286.4(4) Å^3, B_0 = 157(5) GPa, and B_0' = 4(fixed) for zircon structure in YPO_4 nanoparticles and V_0 = 286.7(10) Å^3, B_0 = 156(10) GPa, and B_0' = 4(fixed) for zircon structure in YPO_4:Eu^{3+} nanoparticles. The bulk moduli obtained for zircon phase of our nanoparticles are well-consistent with theoretical estimates[6,29] (Table 1). By refining the XRD patterns from the quenched samples, the unit-cell volume for scheelite YPO_4 and YPO_4Eu^{3+} is also given: V_0= 258.1(3) Å^3 and V_0= 258.8(3) for YPO_4 and YPO_4:Eu^{3+}, respectively.

To verify further the unique phase-transition behavior of YPO_4:Eu^{3+} nanoparticles upon compression, we also conducted high-pressure PL measurements. The PL spectrum of Eu^{3+} ions in YPO_4 at ambient pressure is shown at the bottom of Figure 6a. In zircon YPO_4:Eu^{3+} compounds, the Eu^{3+} ions replace the Y^{3+} ions with D_{2d} site symmetry. Group theory predicts four PL peaks from $^5D_0 \rightarrow {}^7F_{1,2}$ transition in zircon YPO_4:Eu^{3+}; it is widely accepted that $^5D_0 \rightarrow {}^7F_0$ is an electronic transition between nondegenerate levels and has an electric dipole character, and this transition is formally forbidden when the free-ion is considered but is allowed in the solid under certain conditions. Therefore, we take the five peaks from transitions of $^5D_0 \rightarrow {}^7F_{0,1,2}$ as a structure marker at all measured pressures. The two strongest peaks from $^5D_0 \rightarrow {}^7F_1$ transition are located at ~593 and ~597 nm, the emission peaks due to $^5D_0 \rightarrow {}^7F_2$ transition are at ~614 and ~620 nm, and the weak peak at ~581 nm is attributed to $^5D_0 \rightarrow {}^7F_0$ transition.

The pressure evolution of PL spectra up to 43 GPa is depicted in Figure 6a. As seen in this Figure, the most striking feature is that two new emission peaks (at ~615 and ~619 nm) due to $^5D_0 \rightarrow {}^7F_2$ transition become dominant for pressures greater than 23.4 GPa. Meanwhile, the strongest lines due to $^5D_0 \rightarrow {}^7F_1$ transition under ambient conditions decrease in intensity and increase in peak width. Figure 6b shows enlarged PL spectra in the $^5D_0 \rightarrow {}^7F_0$ transition range at various pressures. Beyond 16.8 GPa, the discernible intensity of the peak due to $^5D_0 \rightarrow {}^7F_0$ transition marked with diamond symbols can be enhanced apparently, and the peak position is also altered at the same time. Figure 6c shows the pressure-induced shifts of the PL peaks. Obvious changes in the peak position are clearly shown in the pressure range of 16.8 to 18.4 GPa. Such behavior in PL spectra with increasing pressure suggests that the host materials may undergo a pressure-induced phase transition.

As shown in Figure 6a, it can be found that the most pronounced peaks due to $^5D_0 \rightarrow {}^7F_{1,2}$ transitions in the spectra beyond 23.4 GPa could be presumably attributed to the Eu^{3+} ions with another D_{2d} symmetry. The previous PL studies of YVO_4:Eu^{3+}, $GdVO_4$:Eu^{3+}, and $EuVO_4$ show the zircon-to-scheelite phase transition at high pressure.[16,23,25] However, the PL spectra of YVO_4:Eu^{3+}, $GdVO_4$:Eu^{3+}, and $EuVO_4$ with the scheelite structure show that Eu^{3+} ion is in a distorted D_{2d} symmetry instead of an S_4 symmetry site in the scheelite structure, which can be explained by considering only the first coordination sphere oxygen about the Eu^{3+} ion in an S_4

dx.doi.org/10.1021/jp3088995 | J. Phys. Chem. C 2012, 116, 24837−24844

Table 1. Bulk Modulus (given in GPa) and Unit-Cell Volume at Ambient Pressure (in Å^3) of YPO_4 with Zircon, Monazite, and Scheelite Structure[a]

		bulk modulus		
structure	unit−cell volume	experiments	theory	empirical model
zircon	286.5[b,c]−286.4(4)[e]−286.7(10)[f]	149(2)[b]−186(5)[c]−157(5)[e]−156(10)[f]	144.4[d]−165[c]	143[c]
monazite		206(4)[b]−260[c]	190[c]	
scheelite	258.1(3)[e]−258.8(3)[f]		213.7[c]	

[a]Experimental and theoretical results are included for B_0. [b]Ref 5. [c]Ref 6. [d]Ref 29. [e]Present study for YPO_4 nanoparticles. [f]Present study for YPO_4:Eu^{3+} nanoparticles.

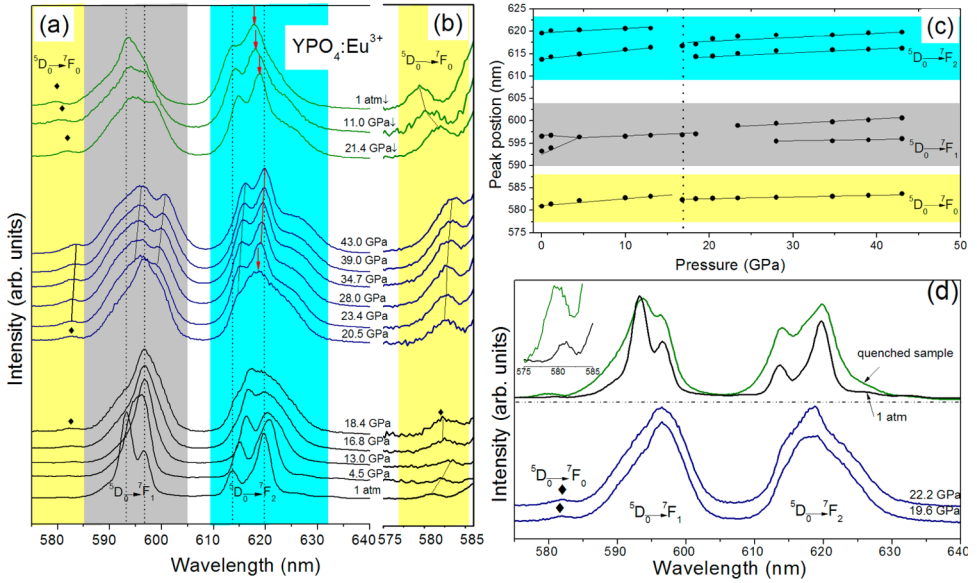

Figure 6. (a) Selected PL spectra of YPO_4:Eu^{3+} nanoparticles at various pressures up to 43 GPa for both compression and decompression processes. (b) Enlarged spectra of panel a in the $^5D_0 \rightarrow {}^7F_0$ transition range. (c) Pressure dependence of the PL peaks. (d) Typical PL spectra of YPO_4:Eu^{3+} nanoparticles up to 22.2 GPa. The inset in panel d shows the $^5D_0 \rightarrow {}^7F_0$ transition of the PL spectra collected under from original and quenched samples enlarged. Different transition ranges are marked with different background colors. Yellow for $^5D_0 \rightarrow {}^7F_0$; gray for $^5D_0 \rightarrow {}^7F_1$; and blue for $^5D_0 \rightarrow {}^7F_2$. The diamonds and arrows denote PL peaks attributed to $^5D_0 \rightarrow {}^7F_0$ and $^5D_0 \rightarrow {}^7F_2$ transitions in the scheelite phase, respectively. The lines are guides for the eyes.

symmetry site in the scheelite structure.[16,23,25] Thus, the scheelite structure is suggested to be the high-pressure phase in the YPO_4:Eu^{3+} nanoparticles.

In fact, it is difficult to see the process of symmetry changes in the pressure range from 18.4 GPa (or even lower, 16.8 GPa) to 23 GPa due to the serious band broadening. Fortunately, for YPO_4 bulk compounds, it has been proved that the zircon-to-monazite transition is reversible and the monazite phase exists in a large pressure range.[5,6] According to the previously proposed phase transformation models by Errandonea et al., the more drastic atomic rearrangement that takes place at the zircon-to-scheelite transition is what makes this transition irreversible while the zircon-to-monazite transition is reversible.[5] Therefore, another high-pressure PL experiment was also conducted. As shown in Figure 6d, although the applied highest pressure is relatively low (22.2 GPa), the peaks due to $^5D_0 \rightarrow {}^7F_{1,2}$ in the quenched sample could be treated as a mixed phase with dominant zircon phase and low-concentration scheelite phase. In the inset of Figure 6d, it is clearly shown that the intensity and position of the peak due to $^5D_0 \rightarrow {}^7F_0$ transition in the quenched sample is changed, implying that high-pressure phase can be reserved from 22.2 GPa. This irreversible behavior reveals the direct zircon-to-scheelite phase transition without the monazite phase. As a whole, the characteristic spectral changes of the YPO_4:Eu^{3+} nanoparticles in the two PL experiments confirm the direct zircon-to-scheelite phase transition, which is consistent with the results observed by high-pressure XRD experiments.

An attempt to gain more insight into the special high-pressure behavior by Raman measurement was unsuccessful due to the very weak Raman signals in DAC. This phenomenon is also observed in bulk YPO_4 sample.[6] Even so, we could gain valuable information from Raman spectra of the quenched samples under ambient conditions, which has gone unnoticed in the work of Zhang et al.[6] The measured Raman spectrum of the original zircon YPO_4:Eu^{3+} nanoparticles is shown in the bottom of Figure 7. Eight peaks could be matched to Raman modes of YPO_4:Eu^{3+} nanoparticles; they are in good agreement with the reported results of bulk crystals.[5,41] One notable discrepancy is the peak observed at ∼421 cm^{-1}. It is likely a second-order Raman mode because a similar phenomenon has been found in bulk YVO_4,[17] $DyVO_4$, and $TbVO_4$.[18] We checked the previous valuable Raman results for the corresponding zircon $RV(P)O_4$ ternary oxides upon compression above all. We find that the internal modes in the $V(P)O_4$, such as $\nu_3(B_g)$, $\nu_3(E_g)$, and $\nu_1(A_g)$ in general drop to lower values in the scheelite phase. In particular, the $\nu_1(A_g)$ mode, which represents the V(P)−O bond stretching mode, is highly sensitive to pressure-induced structural transformations. We list these previous results in Table 2 to make it clear.

dx.doi.org/10.1021/jp3088995 | J. Phys. Chem. C 2012, 116, 24837−24844

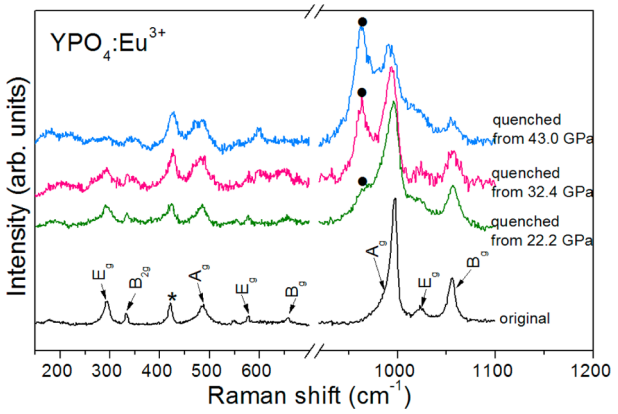

Figure 7. Raman spectra of the ambient sample and the quenched samples from different pressures. The solid circles denote the $\nu_1(A_g)$ mode in scheelite structure.

The Raman spectra of the quenched samples from the high-pressure XRD and PL experiments are shown in Figure 7. In the high-frequency range (920−1100 cm^{-1}), a new mode at 963 cm^{-1} can be detected obviously. As the attainable highest pressure increases, the mode at 963 cm^{-1} gets more and more pronounced, and we could assign it to the $\nu_1(A_g)$ mode of the scheelite phase based on the information listed in Table 2. The $\nu_1(A_g)$ mode at 996 cm^{-1} in zircon phase drops to 963 cm^{-1} in scheelite phase, implying a change in the bond strength. It could be estimated through a simple calculation from the expression for the force constant k because $\nu = 1/2\pi(k/m)^{1/2}$ and $\nu_a^2/\nu_b^2 \approx k_a/k_b$. Therefore, squaring the frequencies and taking their ratio gives a measure of the change in the force constant, which is directly related to the change in the bond strength.[23] Such a calculation shows that there is a 7% decrease in the P−O bond strength in going from zircon to scheelite structure in YPO_4:Eu^{3+} nanoparticles, following the same trend as the reported diffraction measurements of YVO_4.[10]

Multiple factors contribute to the mechanical properties of nanomaterials. A few of studies have reported the nanosized effect could alter phase transformation sequence(s).[42−44] For example, anatase-TiO_2 nanoparticles can directly transform to a second high-pressure phase, baddeleyite structure with the particle size of 12−50 nm or to amorphous phase when the particle size is <10 nm,[42] but in their bulk counterparts, the direct transition to the thermodynamically stable α-PbO_2 structure proceeds above all. It is suggested that the varying surface energy contributions to the total energy of each phase in TiO_2 as a function of crystal size play the crucial roles in the special high-pressure behaviors of phase absence in the processes of structural transitions.[42] As an inevitable fraction of total free energy relative to the bulk counterparts, the higher surface energy contribution in nanomaterials has proven itself successfully and effectively in numerous high-pressure studies to explain the diverse phase stability compared with the bulk.[43−45] With respect to the YPO_4 compounds, we note that there is a competition between the three structures, zircon, monazite and scheelite phase, under high pressure. Therefore, it is expected that higher surface energy attribution to the total energy may have a significant influence on the phase stability. In fact, through theoretical calculations by Zhang et al.,[6] the calculated transition pressures from zircon to monazite phase and from monazite to scheelite phase for YPO_4 are 15.8 and 20.8 GPa, respectively. In other words, the total energy difference between the three phases is theoretically small for YPO_4 in the narrow pressure range of 15.8−20.8 GPa. It is also interesting to note that the direct zircon-to-scheelite phase transition pressure for the YPO_4(:Eu^{3+}) nanoparticles observed in our experiments is ∼18 GPa, which is just located in the narrow pressure range. So for our nanoparticles with the particle size of 50−100 nm it is reasonable to assume that the total energy of different phases under pressure could be altered by nanoscale-induced surface energy difference, enhancing or reducing the stability of corresponding structure(s) relatively. Specifically, the monazite structural stability at high pressure could be relatively reduced, making it more unstable than that of either zircon or scheelite phase, resulting in the direct zircon-to-scheelite transition without going through monazite structure. As we discussed in the aforementioned section, the effects from dopants and quasi-hydrostatic stress could not play crucial roles in the distinctive high-pressure behavior of the nanoparticles. In addition, size-dependent defect ratio, stress distribution, and shape effect have been used to explain the diverse structural stability and different phase transformation behaviors of bulk and nano ZnS, MnS, and $CuGaS_2$,[43,45−48] but

Table 2. Overview of the Experimental Raman V(P)−O Bond Stretching Frequencies (cm^{-1}) from the Reported Bulk Samples by High-Pressure Raman Scattering Measurements under Ambient Conditions and from the Quenched Samples in $RV(P)O_4$

zircon				scheelite		
$\nu_3(B_g)$	$\nu_3(E_g)$	$\nu_1(A_g)$	crystal/[ref]	$\nu_3(E_g)$	$\nu_3(B_g)$	$\nu_1(A_g)$
828.3	828.7	872.3	$CeVO_4$/[7]	772.6	817.1	840.26
811	827	887	$GdVO_4$/[16]	745	804	833
807	824	883	$TbVO_4$/[18]	742	802	829
810	827	886	$DyVO_4$/[18]	741	801	825
816	838.8	891.1	YVO_4/[17]	747.8	812.7	829.4
823	842	898	$YbVO_4$/[20]	761	813	820
825	845	899	$LuVO_4$/[14]	779	787	853
817.1	856.5	914.2	$ScVO_4$/[15]	727.5	760.9	826.1
1064	1027	1006	$TmPO_4$/[3]	1027(10)	1063(13)	987(8)
948	969	1006	$TbPO_4$/[13]			

Monazite								
cystal/[ref]	B_g	A_g	A_g	B_g	A_g	B_g	B_g	A_g
$TbPO_4$/[13]	968	1005	1033	1040	1070	1080	1093	
$CeVO_4$/[7]	817.2	801.3	825.3	862.1	853.3	872.8	903.7	873.8

dx.doi.org/10.1021/jp3088995 | J. Phys. Chem. C 2012, 116, 24837−24844

these factors originate mainly from finite size (<15 nm) or special morphology (such as nanobelt and nanorod), whereas the nano YPO_4(:Eu^{3+}) samples (particle-like and 50−100 nm in diameter) in this study do not have these features. Therefore, it is inappropriate to explain the special phase-transition route in the YPO_4(:Eu^{3+}) nanoparticles by these factors. In summary, we propose that the nanoscale-induced surface energy difference would be the dominant factor, leading to the special phase-transition behavior in the YPO_4 nanoparticles. To our best knowledge, it is the first study to show that the nanoscale-induced effect could alter the phase-transition routes on the ternary oxides compared with the bulk, which may lead to a deeper understanding of the mechanical properties of nanomaterials.

Size selectivity in nanocrystals is of fundamental significance to search for new structural materials with new properties. However, determining the critical size requires a number of starting nanomaterials representing a spread of average crystallite size with small size dispersions. In view of this, further research work on development of synthetic strategies and routes of the corresponding nanomaterials is necessary to understand this issue. Zircon YPO_4 nanoparticles could "jump" the metastable monazite phase and transform to the scheelite phase directly by the virtue of nanoscale-induced higher surface energy contribution, lowering the transition pressure for generation of the scheelite phase compared with the bulk. From the viewpoint of practical application, this reduction of phase-transition pressure means that one may gain new structural materials under less "tough" conditions, relatively low pressure, if the final-state materials with high-pressure phase could be reserved upon complete decompression. Therefore, compression of these starting compounds on the nanoscale is suggested as an optimizing feasible synthetic path to fabrication of new structural technologically relevant materials with tailored properties.

CONCLUSIONS

In summary, we have investigated the high-pressure structures and properties of the particle-like nanostructured YPO_4 and YPO_4:Eu^{3+} samples using XRD and PL measurements. The phase-transition sequence of the nanoparticles is zircon phase → scheelite phase (∼18 GPa), in contrast with the phase transition of zircon phase → monazite phase (∼15 GPa) → scheelite phase (∼30 GPa) in bulk YPO_4.[6] Through refining the different XRD patterns, the bulk moduli have been obtained for the zircon phase of our nanoparticles, and the results are well-consistent with theoretical estimates. In addition, the valuable Raman mode $\nu_1(A_g)$ (at 963 cm^{-1}) of the scheelite phase is identified. By a simple calculation, it is estimated that there is a 7% decrease in the P−O bond strength in going from zircon to scheelite structure in the nanoparticles. Finally, it is proposed that the nanoscale-induced higher surface energy contribution plays a crucial role in the unusual high-pressure behavior of the YPO_4 and YPO_4:Eu^{3+} nanoparticles. This study offers important information on the optimizing fabrication of new structural functional materials by virtue of nanoscale-induced effect.

AUTHOR INFORMATION

Corresponding Author

*E-mail: zoubo@jlu.edu.cn.

Notes

The authors declare no competing financial interest.

ACKNOWLEDGMENTS

This work is supported by NSFC (nos. 21073071, 11204101 and 51025206), National Basic Research Program of China (no. 2011CB808200), Changjiang Scholar and Innovative Research Team in University (No. IRT1132), and the Graduate Innovation Fund of Jilin University (no. 20121041). Angle-dispersive XRD measurement was performed at beamline 15U1 at the Shanghai Synchrotron Radiation Facility (SSRF).

REFERENCES

(1) Errandonea, D.; Javier Manjón, F. *Prog. Mater Sci.* **2008**, *53*, 711−773.
(2) Finch, R. J.; Hanchar, J. M. *Rev. Miner. Geochem.* **2003**, *53*, 1−25.
(3) Stavrou, E.; Tatsi, A.; Raptis, C.; Efthimiopoulos, I.; Syassen, K.; Muñoz, A.; Rodríguez-Hernández, P.; López-Solano, J.; Hanfland, M. *Phys. Rev. B* **2012**, *85*, 024117-1−024117-12.
(4) López-Solano, J.; Rodríguez-Hernández, P.; Muñoz, A.; Gomis, O.; Santamaría-Perez, D.; Errandonea, D.; Manjón, F. J.; Kumar, R. S.; Stavrou, E.; Raptis, C. *Phys. Rev. B* **2010**, *81*, 144126-1−144126-9.
(5) Lacomba-Perales, R.; Errandonea, D.; Meng, Y.; Bettinelli, M. *Phys. Rev. B* **2010**, *81*, 064113-1−064113-9.
(6) Zhang, F. X.; Wang, J. W.; Lang, M.; Zhang, J. M.; Ewing, R. C.; Boatner, L. A. *Phys. Rev. B* **2009**, *80*, 184114-1−184114-7.
(7) Panchal, V.; Lopez-Moreno, S.; Santamaria-Perez, D.; Errandonea, D.; Manjón, F. J.; Rodriguez-Hernandez, P.; Munoz, A.; Achary, S. N.; Tyagi, A. K. *Phys. Rev. B* **2011**, *84*, 024111-1−024111-12.
(8) Errandonea, D.; Kumar, R. S.; Achary, S. N.; Tyagi, A. K. *Phys. Rev. B* **2011**, *84*, 224121-1−224121-8.
(9) Errandonea, D.; Lacomba-Perales, R.; Ruiz-Fuertes, J.; Segura, A.; Achary, S. N.; Tyagi, A. K. *Phys. Rev. B* **2009**, *79*, 184104-1−184104-9.
(10) Wang, X.; Loa, I.; Syassen, K.; Hanfland, M.; Ferrand, B. *Phys. Rev. B* **2004**, *70*, 064109-1−064109-6.
(11) Errandonea, D.; Kumar, R.; Lopez-Solano, J.; Rodriguez-Hernandez, P.; Munoz, A.; Rabie, M. G.; Saez Puche, R. *Phys. Rev. B* **2011**, *83*, 134109-1−134109-12.
(12) Zhang, F. X.; Lang, M.; Ewing, R. C.; Lian, J.; Wang, Z. W.; Hu, J.; Boatner, L. A. *J. Solid State Chem.* **2008**, *181*, 2633−2638.
(13) Tatsi, A.; Stavrou, E.; Boulmetis, Y.; Kontos, A.; Raptis, Y.; Raptis, C. *J. Phys.: Condens. Matter* **2008**, *20*, 425216-1−425216-7.
(14) Rao, R.; Garg, A. B.; Sakuntala, T.; Achary, S.; Tyagi, A. *J. Solid State Chem.* **2009**, *182*, 1879−1883.
(15) Panchal, V.; Manjón, F. J.; Errandonea, D.; Rodriguez-Hernandez, P.; Lopez-Solano, J.; Munoz, A.; Achary, S. N.; Tyagi, A. K. *Phys. Rev. B* **2011**, *83*, 064111-1−064111-10.
(16) Zhang, C. C.; Zhang, Z. M.; Dai, R. C.; Wang, Z. P.; Zhang, J. W.; Ding, Z. J. *J. Phys. Chem. C* **2010**, *114*, 18279−18282.
(17) Manjón, F. J.; Rodríguez-Hernández, P.; Muñoz, A.; Romero, A. H.; Errandonea, D.; Syassen, K. *Phys. Rev. B* **2010**, *81*, 075202-1−075202-11.
(18) Duclos, S. J.; Jayaraman, A.; Espinosa, G.; Cooper, A.; Maines, R., Sr *J. Phys. Chem. Solids* **1989**, *50*, 769−775.
(19) Jayaraman, A.; Kourouklis, G.; Espinosa, G.; Cooper, A.; Van Uitert, L. *J. Phys. Chem. Solids* **1987**, *48*, 755−759.
(20) Garg, A. B.; Rao, R.; Sakuntala, T.; Wani, B.; Vijayakumar, V. *J. Appl. Phys.* **2009**, *106*, 063513-1−063513-6.
(21) Stavrou, E.; Tatsi, A.; Salpea, E.; Boulmetis, Y.; Kontos, A.; Raptis, Y.; Raptis, C. *J. Phys.: Conf. Ser.* **2008**, *121*, 042016-1−042016-6.
(22) Manjón, F. J.; Jandl, S.; Riou, G.; Ferrand, B.; Syassen, K. *Phys. Rev. B* **2004**, *69*, 165121−1−165121−7.
(23) Chen, G.; Stump, N.; Haire, R.; Peterson, J.; Abraham, M. *Solid State Commun.* **1992**, *84*, 313−315.
(24) Chen, G.; Hölsä, J.; Peterson, J. *J. Phys. Chem. Solids* **1997**, *58*, 2031−2037.

(25) Chen, G.; Haire, R.; Peterson, J.; Abraham, M. *J. Phys. Chem. Solids* **1994**, *55*, 313−316.
(26) Flórez, M.; Contreras-García, J.; Recio, J. M.; Marqués, M. *Phys. Rev. B* **2009**, *79*, 104101-1−104101-11.
(27) Smirnov, M. B.; Mirgorodsky, A. P.; Kazimirov, V. Y.; Guinebretière, R. *Phys. Rev. B* **2008**, *78*, 094109-1−094109-11.
(28) Bose, P. P.; Mittal, R.; Chaplot, S. L. *Phys. Rev. B* **2009**, *79*, 174301-1−174301-8.
(29) Li, H. Y.; Zhang, S. Y.; Zhou, S. H; Cao, X. Q. *Inorg. Chem.* **2009**, *48*, 4542−4548.
(30) Kolitsch, U.; Holtstam, D. *Eur. J. Mineral.* **2004**, *16*, 117−126.
(31) San-Miguel, A. *Chem. Soc. Rev.* **2006**, *35*, 876−889.
(32) Zhu, H. L.; Yang, H.; Jin, D. L.; Wang, Z. K.; Gu, X. Y.; Yao, X. H.; Yao, K. H. *J. Nanopart. Res.* **2008**, *10*, 1149−1154.
(33) Zhu, H. L.; Zuo, D. T. *J. Phys. Chem. C* **2009**, *113*, 10402−10406.
(34) Mao, H. K.; Xu, J.; Bell, P. *J. Geophys. Res.* **1986**, *91*, 4673−4676.
(35) Hammersley, A.; Svensson, S.; Hanfland, M.; Fitch, A.; Hausermann, D. *High Pressure Res.* **1996**, *14*, 235−248.
(36) Larson, A. C.; Von Dreele, R. B. *General Structure Analysis System (GSAS)*; Los Alamos National Laboratory Report LAUR 86-748, 2004.
(37) Zhao, X. G.; Yan, T. T.; Wang, K.; Yan, Y.; Zou, B.; Yu, J. H.; Xu, R. R. *Eur. J. Inorg. Chem.* **2012**, *2012*, 2527−2532.
(38) Dong, Y. J.; Xu, B.; Zhang, J. B.; Tan, X.; Wang, L. J.; Chen, J. L.; Lv, H. G.; Wen, S. P.; Li, B.; Ye, L.; Zou, B.; Tian, W. J. *Angew. Chem., Int. Ed.* **2012**, *51*, 10782−10785.
(39) Zhao, X. G.; Wang, K.; Yan, T. T.; Yan, Y.; Zou, B.; Yu, J. H.; Xu, R. R. *Chin. J. Chem.* **2012**, *30*, 2066−2072.
(40) Wang, L.; Pan, Y.; Ding, Y.; Yang, W.; Mao, W. L.; Sinogeikin, S. V.; Meng, Y.; Shen, G.; Mao, H. *Appl. Phys. Lett.* **2009**, *94*, 061921-1−061921-3.
(41) Giarola, M.; Sanson, A.; Rahman, A.; Mariotto, G.; Bettinelli, M.; Speghini, A.; Cazzanelli, E. *Phys. Rev. B* **2011**, *83*, 224302-1−224302-8.
(42) Swamy, V.; Kuznetsov, A.; Dubrovinsky, L. S.; Caruso, R. A.; Shchukin, D. G.; Muddle, B. C. *Phys. Rev. B* **2005**, *71*, 184302-1−184302-11.
(43) Wang, Z. W.; Daemen, L. L.; Zhao, Y. Z.; Zha, C. S.; Downs, R. T.; Wang, X. D; Wang, Z. L.; Hemley, R. J. *Nat. Mater.* **2005**, *4*, 922−927.
(44) Lv, H.; Yao, M. G.; Li, Q. J.; Li, Z. P.; Liu, B.; Liu, R.; Lu, S. C.; Li, D. M.; Mao, J.; Ji, X. L.; Liu, J.; Chen, Z. Q.; Zou, B.; Cui, T.; Liu, B. B. *J. Phys. Chem. C* **2012**, *116*, 2165−2171.
(45) Wang, Z. W.; Guo, Q. *J. Phys. Chem. C* **2009**, *113*, 4286−4295.
(46) Li, Z. P.; Liu, B. B.; Yu, S. D.; Wang, J. H.; Li, Q. J.; Zou, B.; Cui, T.; Liu, Z. X.; Chen, Z. Q.; Liu, J. *J. Phys. Chem. C* **2011**, *115*, 357−361.
(47) Yang, X. Y.; Wang, Y. N.; Wang, K.; Sui, Y. M.; Zhang, M. G.; Li, B. B.; Ma, Y. M.; Liu, B.; Zou, G. T.; Zou, B. *J. Phys. Chem. C* **2012**, *116*, 3292−3297.
(48) Xiao, N. R.; Zhu, L.; Wang, K.; Dai, Q. Q.; Wang, Y. N.; Li, S. R.; Sui, Y. M.; Ma, Y. M.; Liu, J.; Liu, B. B.; Zou, G. T.; Zou, B. *Nanoscale* **2012**, DOI: 10.1039/C2NR31629C.